Translational and rotational resonance frequencies of a disk in a single-axis acoustic levitator

Sílvio L. Vieira[1,a)], Marco A. B. Andrade[2]

[1]Institute of Physics, Federal University of Goiás, Goiânia 74690-900, Brazil

[2]Institute of Physics, University of São Paulo, São Paulo 05508-090, Brazil

[a)]Author to whom correspondence should be addressed. Electronic mail: slvieira@ufg.br

Abstract: In this study, we investigate the acoustic levitation of a disk in a single-axis acoustic levitator operating at 21.53 kHz. First, two acoustic models based on the Finite Element Method are employed for calculating the acoustic radiation force and torque on a levitating disk. The models are also used for calculating the vertical, horizontal and torsional trapping stiffness and its corresponding natural frequencies. Furthermore, translational and angular oscillations of the disk are captured by a high-speed camera and a tracking algorithm is employed for extracting the natural frequencies of the oscillations. The experimental natural frequencies present good agreement with those predicted by the models. Although the numerical model was employed for simulating the forces and torques on a disk, the presented method is general and it can be employed for simulating the acoustic levitation of objects of arbitrary shapes and sizes.

I. INTRODUCTION

Acoustic levitation[1–4] has emerged as a promising tool for many applications, ranging from chemistry[5,6], pharmacy[7,8] and biology[9–12] to the handling of delicate components[13–15]. Acoustic levitation relies on the phenomenon of acoustic radiation force[16,17] and allows the contactless support of a wide variety of materials, such as liquids[4,18,19], solids[14,20], soap bubbles[21] and even small insects[22,23].

Acoustic levitation is usually achieved either by a single-axis acoustic levitator[24–27] or using arrays of low power ultrasonic transducers[28–37]. Acoustic levitators based on arrays of low power transducer offer greater flexibility, allowing the levitation and the controlled manipulation of small objects in three-dimensions. However, they require complex electronics to control the phases of each transducer individually[28,38]. A single-axis acoustic levitator basically consists of an ultrasonic transducer and an opposing reflector, which are separated by such a distance that a resonant standing wave is generated between them. The standing wave has a series of pressure nodes in which objects of positive acoustic contrast factor are stably trapped due to the action of the acoustic radiation force. Because of its simplicity, single-axis levitators are widely used in combination with remote detection methods (e.g. Raman spectroscopy, X-ray diffraction) for analyzing levitating samples[9,12,39–41].

In the recent years, many advances have been made in the development of acoustic levitation devices. New levitation systems allow contactless manipulation capability in one[42], two[32,33,43] and three[28,29] dimensions and now acoustic levitation is no longer restricted to objects smaller than the acoustic wavelength[31,34,44]. Distinct holographic techniques have also been proposed to generate complex acoustic fields[29,45,46] and to allow multiple objects to be manipulated independently[35]. The manipulation speed has also increased from few millimeters per second to several meters per second. In a recent experiment[47], expanded polystyrene particles have been manipulated with a speed of up to 8.75 m/s.

In general, acoustic levitation devices are simulated by using a numerical method to find the acoustic pressure and velocity fields. Then these fields are replaced into the well-known Gor'kov equation[48] to obtain the potential of the acoustic radiation force that acts on the levitating object. Although this approach has been widely used in many studies[26,29,32,33,43,49,50], it has some simplifications that can lead to an incorrect evaluation of the acoustic radiation force. First, the Gor'kov equation is only valid for objects much smaller than the acoustic wavelength. Second, the Gor'kov equation assumes that the radiation force is described in terms of a potential, which is only valid for conservative forces[51]. Finally, in this approach the pressure and velocity fields are simulated without the presence of the object, and thus it does not capture the fact the presence of the object affects

the resonance frequency of the levitator[52,53]. In addition to these limitations, many applications involve the acoustic levitation of larger non-spherical objects, which cannot be considered much smaller than the acoustic wavelength. For non-spherical objects, such as disks[54,55], cubes[20] and octahedrons[34], the levitator must provide not only a restoring acoustic radiation force to trap the object in position, but also a restoring torque to trap the object in orientation.

In this paper, the acoustic radiation force and the acoustic radiation torque acting on a levitating disk of finite size is investigated numerically and experimentally. A disk is chosen because it has a simple geometry and its analysis can be easily extended to objects of more complex geometries. The disk is levitated by a single-axis acoustic levitator consisting of a Langevin-type transducer and an opposing reflector. The forces and torques acting on the disk are simulated by using the Finite Element Method (FEM). The FEM model is also used for calculating the vertical, horizontal and torsional trapping stiffness. Experiments with a high-speed camera are carried out to obtain the natural frequencies of the vertical, horizontal and angular oscillations of the disk.

II. EXPERIMENTAL SETUP

The acoustic levitation of a disk is investigated using the experimental setup illustrated in Fig. 1. A polyacetal disk of 3.1 mm radius, 2 mm thickness, and a mass of 85 mg, which was machined in a lathe, is suspended by a single-axis acoustic levitator consisting of a Langevin-type transducer and an opposing aluminum reflector. The transducer operates at a frequency of 21.53 kHz, and it has a plane radiating surface of 31 mm in diameter. The transducer radiating surface is located at a distance H from a plane reflector of 38 mm in diameter. The reflector is positioned on the pan of an electronic precision scale (UX420H, Shimadzu, Japan) and kept at a fixed position, whereas the transducer can move up and down by a motorized stage. The precision scale measures the acoustic radiation force on the reflector as a function of the transducer-reflector distance H.

In all the experiments, the transducer is excited with a sine wave of 21.53 kHz, which is generated by a function generator (33512B, Keysight Technologies, USA) and amplified by a high-power amplifier (700A1, Amplifier Research Corp., USA). The levitation experiments are carried out with the levitator operating under the third resonance mode ($H \approx 3\lambda/2$, where λ is the acoustic wavelength), thus generating a standing wave with three pressure nodes between the transducer and the reflector.

Translational and angular oscillations of the levitating disk are recorded by a high-speed camera (FASTCAM Mini UX50, Photron, Japan). As shown in Fig. 1, the camera is positioned transversally to the levitated object and against a light diffuser background. Vertical oscillations of the disk are

induced by switching the voltage amplitude applied to the transducer. This rapid switch of the voltage amplitude changes the disk equilibrium position, which causes the disk to oscillate about its equilibrium position. Angular and horizontal oscillations are induced through manual perturbation using a pair of tweezers. The resulting oscillations of the position and tilt angle as a function of time were recorded by the high-speed camera. A script written in the software MATLAB (MathWorks Inc., Natick, MA, USA) is used to track the position of the center of mass and tilt angle as a function of time.

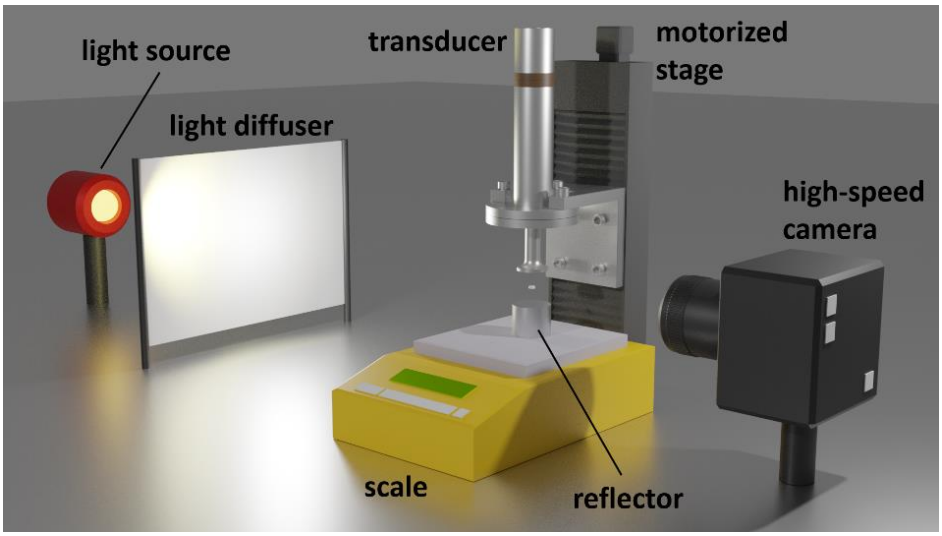

FIG. 1. Illustration of the experimental setup.

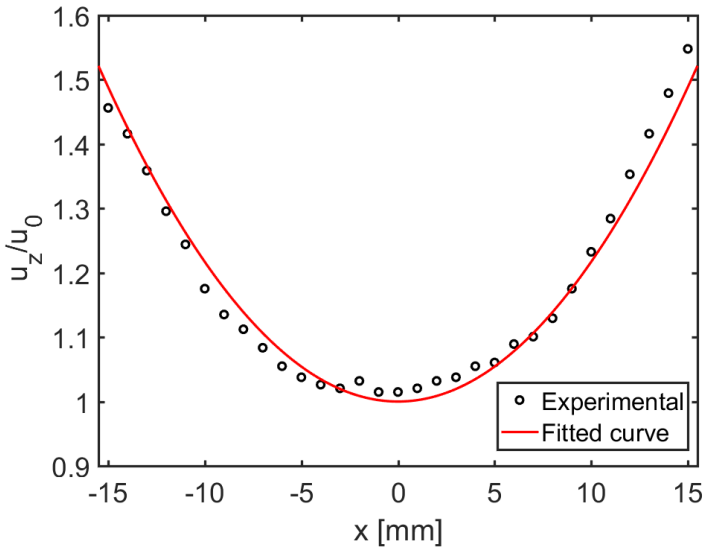

FIG. 2. Displacement amplitude along the transducer radiating surface measured by a Laser Doppler Vibrometer.

The radiation surface of transducer presents a non-uniform vibration pattern, with a minimum displacement amplitude at its center and maximum displacement amplitude at the edges. The transducer displacement amplitude distribution along the transducer surface was measured by a single-point Laser Doppler Vibrometer (OFV-534 Sensor Head with an OFV-5000 controller, Polytec GmbH, Germany). The displacement amplitude measurements were made along a straight line passing through the center of the transducer in steps of 1 mm. As shown in Fig. 2, the displacement amplitude u_z along the transducer surface depends on the radial coordinate $r = \sqrt{x^2 + y^2}$ and it can be approximated by

$$u_z(r) = u_0(1 + \beta r^2), \tag{1}$$

where u_0 is the displacement amplitude at the center and the constant β = 2.171 x 10^3 m^{-2} was obtained by fitting a parabola to the measured data (Fig. 2).

III. NUMERICAL MODELS

The acoustic levitation of a disk is simulated using the Finite Element Method (FEM) software COMSOL Multiphysics (COMSOL AB, Stockholm, Sweden).

Two acoustic models based on the linear wave equation are employed for simulating the acoustic pressure p and particle velocity **v** fields in the air gap between the transducer and the reflector. These fields are then used for calculating the radiation force and the radiation torque on a levitating disk of thickness h = 2 mm and radius a = 3.1 mm. An axisymmetric model [Fig. 3(a)] simulates the vertical radiation force F_z on the disk as a function of its vertical position z, whereas the horizontal force F_x and the y-component of the acoustic radiation torque vector $\boldsymbol{\tau}$ are simulated using the 3D acoustic model of Fig. 3(b). The horizontal force F_x and the torque τ_y are calculated as a function of the horizontal disk position x and tilt angle θ, respectively.

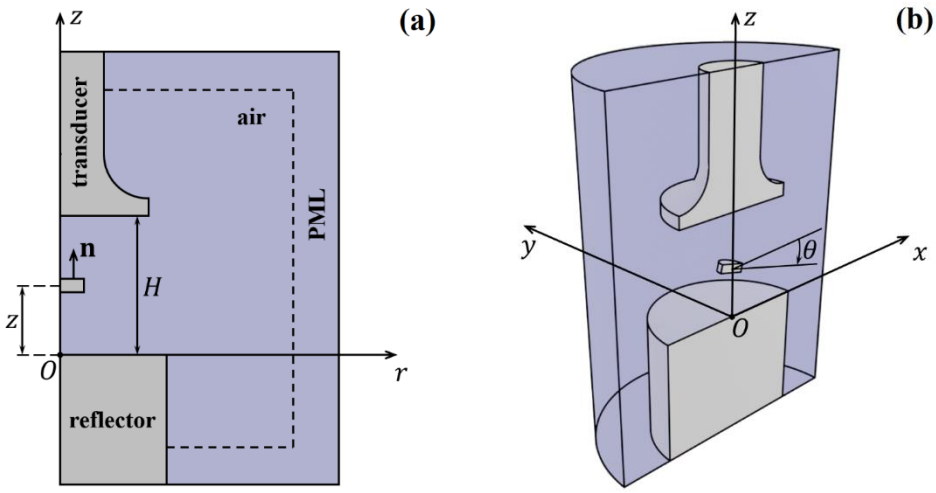

FIG. 3. Numerical acoustic models used for simulating the acoustic radiation force and the acoustic radiation torque on a levitating disk. (a) Axisymmetric model. (b) Three-dimensional acoustic numerical model. Because of the symmetry in respect to the xz-plane, only half of the geometry was considered in the 3D simulation and a symmetry boundary condition was applied over the xz-plane.

The free space between the transducer and the reflector is defined as an air domain, which has a density of ρ_0 = 1.2 kg/m^3 and a sound velocity of c_0 = 349 m/s. For the axisymmetric model of Fig. 3(a), the air domain was meshed with approximately 9000 triangular elements of 0.4 mm at the disk surface and 1 mm at the edges of the air domain. For the 3D model [Fig. 3(b)], around 475000 tetrahedral elements are employed to simulate the air domain, with a mesh size of 0.2 mm at the disk surface and 1.4 mm at the outer edges. A special air absorbing layer is simulated using a Perfectly Matched Layer (PML) to prevent wave reflections of the outgoing acoustic waves at the boundaries of the air domain. The reflector and disk are considered to be impenetrable to sound waves, leading to the boundary condition $\mathbf{n} \cdot \nabla p = 0$ at the air-reflector and air-disk interfaces, where $\mathbf{n}$ is the unit normal vector to the surface. The acoustic waves are generated by assuming that the displacement amplitude along the transducer surface is given by Eq. (1).

Instead of using the Gor'kov equation, the acoustic radiation force $\mathbf{F}$ on the disk is calculated by integrating the acoustic radiation pressure over the disk surface [3,16,56]:

$$\mathbf{F} = -\int_{S_0} \langle p_{rad} \rangle \mathbf{n} dS, \tag{2}$$

where $\mathbf{n}$ is the outward normal vector and the integral is evaluated over the object surface S_0. In Eq. (2), the time-average acoustic radiation pressure $\langle p_{rad} \rangle$ is given by

$$\langle p_{rad} \rangle = \frac{1}{2\rho_0 c_0^2} \langle p^2 \rangle - \frac{\rho_0}{2} \langle \mathbf{v} \cdot \mathbf{v} \rangle, \tag{3}$$

in which the angle brackets ⟨ ⟩ represent the time-average.

The acoustic radiation torque $\boldsymbol{\tau}$ on the disk is calculated by[57],

$$\boldsymbol{\tau} = -\int_{S_0} \langle p_{rad} \rangle \mathbf{r} \times \mathbf{n} dS, \tag{4}$$

where the vector $\mathbf{r}$ points from the center of mass to a point on the surface of the object.

The dynamic response of a levitated object for small displacements in respect to its equilibrium position is analogous to the behavior of a harmonic oscillator[58–61]. In this analysis, we neglect viscosity and assume an undamped motion of the levitated object. Accordingly, an elastic constant can be defined as

$$k_z = -\frac{\partial F_z}{\partial z}, \tag{5}$$

$$k_x = -\frac{\partial F_x}{\partial x}. \tag{6}$$

In Eqs. (5) and (6), k_z and k_x are the vertical and horizontal trapping stiffness, respectively. Similarly, the torsional constant k_y^{rot} for the disk rotation around the y-axis can be calculated by

$$k_y^{rot} = -\frac{\partial \tau_y}{\partial \theta}. \tag{7}$$

Using the elastic and torsional constants, the natural frequencies of the vertical and horizontal oscillations are calculated by

$$f_z = \frac{1}{2\pi}\sqrt{\frac{k_z}{m}}, \tag{8}$$

$$f_x = \frac{1}{2\pi}\sqrt{\frac{k_x}{m}}, \tag{9}$$

and the natural frequency for angular oscillations of the disk is given by

$$f_y^{rot} = \frac{1}{2\pi}\sqrt{\frac{k_y^{rot}}{I}}, \tag{10}$$

where I is the disk's moment of inertia for rotations about the y direction, given by

$$I = m(3a^2 + h^2)/12. \tag{11}$$

It is interesting to mention that the trapping stiffness given by Eqs. (5), (6) and (7) are proportional to the voltage amplitude squared. As a consequence, the natural frequencies given by Eqs. (8), (9) and (10) are proportional the excitation voltage. This means that, in contrast with a spring-mass system in which the spring stiffness is constant, the natural frequency can be altered by changing the voltage amplitude applied to the transducer.

IV. RESULTS AND DISCUSSION

Before conducting the levitation experiments, the resonances (i.e. the values of H in which the acoustic pressure is maximized) of the empty levitator were found by measuring the acoustic radiation force on the reflector as a function of H. For a plane standing wave field, the resonances would occur for $H_n = n\lambda/2$ (n = 1, 2, 3, …). However, the wave inside a real levitator is not plane[49] and the resonance distances occur when H_n are slightly greater than $n\lambda/2$. Consequently, the resonance distance H_n of a state n is found by identifying the peaks in the force-distance curve[62].

The acoustic radiation force on the reflector was also simulated using the FEM model of Fig. 3(a) without the presence of the disk. The model calculates the acoustic pressure and the particle velocity distributions in the air medium and the force on the reflector is obtained by integrating the time-average acoustic radiation pressure over the reflector surface. In this simulation, we assumed u_0 = 2.65 μm. This value was found by making the first simulated peak to coincide with the first measured peak. Because of this normalization procedure, the absolute force values should be interpreted qualitatively. Moreover, the experiments were carried out the levitator operating with a high acoustic pressure amplitude, resulting in harmonic generation due to the nonlinear wave propagation[63,64]. Since the model is based on the linear wave equation, it does not capture the influence of harmonic generation on the radiation force.

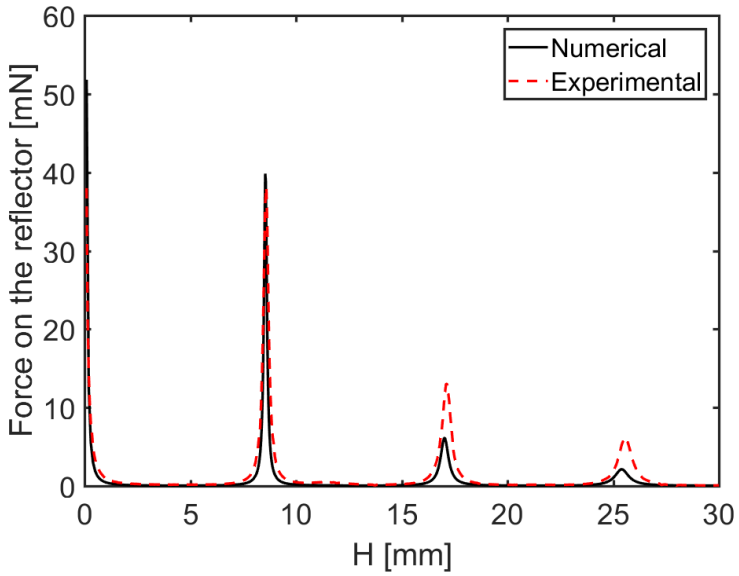

FIG. 4. Acoustic radiation force on the reflector versus H for an empty levitator. The force was simulated by assuming u_0 = 2.65 μm at the center of the transducer.

The comparison between the experimental and simulated forces on the reflector is shown in Fig. 4. The peaks of the experimental curve occur at H_1 = 8.60 ± 0.12 mm, H_2 = 17.10 ± 0.16 mm and H_3 = 25.60 ± 0.21 mm, whereas the peaks of the numerical curve occur at $H_1 = 0.528\lambda$ = 8.55 mm, $H_2 = 1.052\lambda$ = 17.05 mm and $H_3 = 1.567\lambda$ = 25.40 mm. The uncertainties of H_n were found by combining an estimated systematic error of 0.1 mm in the transducer-reflector distance with the uncertainty in the speed of sound (≈ 1.2 m/s) caused by temperature fluctuations. The experiments were carried out a room temperature (39 ± 2 ºC) with no temperature control.

The acoustic levitation of a polyacetal disk is investigated with the levitator operating under the third resonance (n = 3), which generates a standing wave with three pressure nodes between the transducer and the reflector. In all the levitation experiments, the disk is inserted in the middle pressure node with a pair of tweezers. Although the maximum pressure amplitude is achieved at the resonance (H_3 = 25.6 mm), we were unable to levitate the disk when the transducer-reflector distance was set to 25.6 mm. When operating the levitator at the resonance, the disk is subjected to oscillational instability[65,66], causing the disk to oscillate vertically. As investigated in a previous study[65], a time delay in the response of the acoustic cavity can lead to three different behaviors of the levitating object. If the transducer-reflector distance H is slightly less than the resonant distance, the levitation is stable. When H is set to a small interval in the neighborhood of a resonant state, the object oscillates vertically with constant amplitude. For H above the resonant state, the oscillation amplitude increases

exponentially until the object is ejected out of the levitator. Therefore, the transducer-reflector distance was reduced to H = 25.0 mm in order to achieve a stable levitation.

The comparison between the simulated acoustic pressure distribution and a picture of the levitating disk is shown in Fig. 5. The simulation was carried out using the axisymmetric model of Fig. 3(a). It was assumed the non-uniform displacement profile given by Eq. (1), with displacement amplitude of 5.6 µm at the center of the transducer. For this transducer displacement amplitude, the disk equilibrium position is z_{eq} = 11.95 mm. The equilibrium position occurs when the gravitational force acting on the disk ($F_g = mg$ = 833.8 µN, where m = 85 mg is the disk mass and g = 9.81 m/s^2 is the gravitational acceleration) is counterbalanced by the opposing radiation force F_z. In the FEM model, the equilibrium position was found by simulating the acoustic radiation force on the disk as a function of its vertical position z and then finding the disk vertical position in which $F_g = F_z$, resulting in z_{eq} = 11.95 mm.

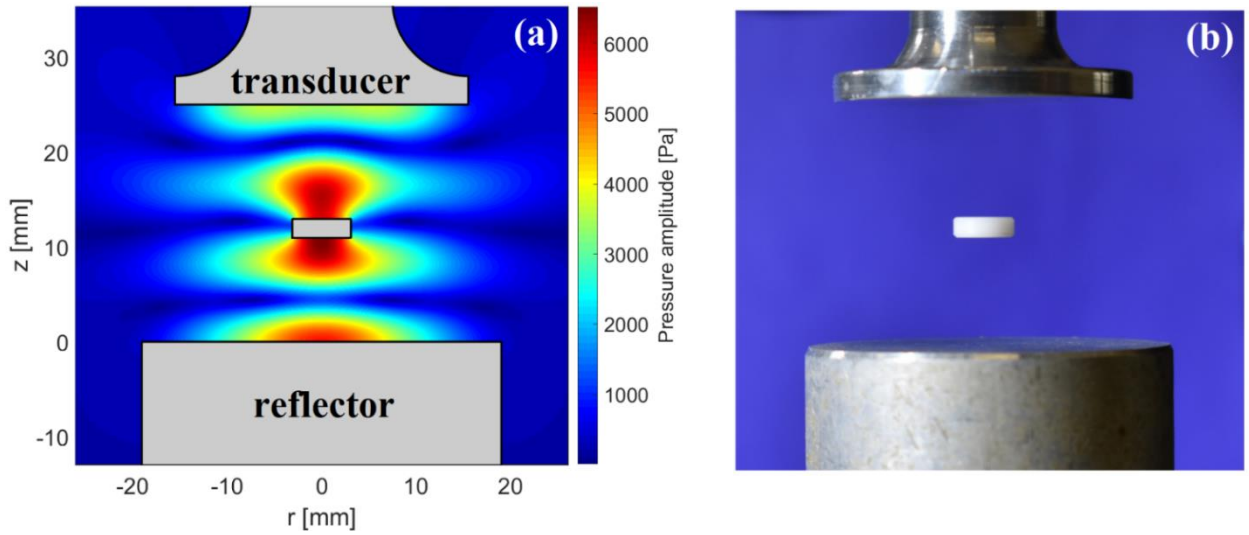

FIG. 5. Comparison between the acoustic pressure field and the levitation position of a polyacetal disk for a transducer-reflector distance H = 25.0 mm and the transducer oscillating at 21.53 kHz, with a displacement amplitude u_0 = 5.6 µm at its center. (a) Numerical simulation (axisymmetric model). (b) Experiment.

The axisymmetric FEM model of Fig. 3(a) was also employed to calculate the acoustic radiation forces on the reflector [Fig. 6(a)] and on the disk [Fig. 6(b)] as a function of the disk vertical position z. It is interesting to note that the acoustic radiation force on the reflector [Fig. 6(a)] varies with the disk position. This change is caused by the wave scattered by the disk, which depends on the size and position of the object. For a levitator operating at a constant frequency and a fixed separation between the transducer and the reflector, the acoustic pressure distribution inside the levitator varies

with the disk position, causing a change in the radiation force on the reflector. The maximum forces on the reflector occur when the disk is located at the pressure nodes of the standing wave.

The simulated radiation force on the disk as a function of its vertical position is shown in Fig. 6(b). This figure also presents the tangent line at the equilibrium position z_{eq} = 11.95 mm. Using Eq. (5), we obtain an elastic constant k_z = 1.31 N/m at the disk equilibrium position. By replacing this elastic constant into Eq. (8), we obtain f_z = 19.76 Hz for the vertical oscillations of the disk in respect to its equilibrium position.

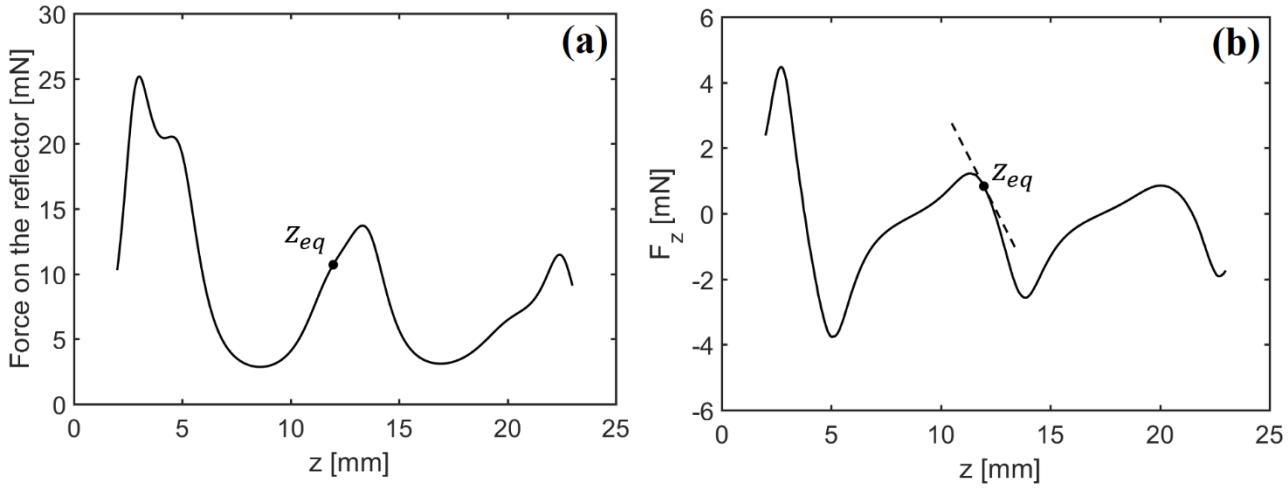

FIG. 6. Simulated acoustic radiation force on the reflector and on the disk as a function of the disk vertical position: (a) Force on the reflector. (b) Vertical radiation force F_z on the disk. The results were obtained for the transducer operating at 21.53 kHz with displacement amplitude u_0 = 5.6 µm and a transducer-reflector distance of 25.0 mm. For the disk levitating at the middle pressure node, the equilibrium position corresponds to z_{eq} = 11.95 mm.

Because of the circular symmetry, the disk is only subjected to vertical forces when it is located along the z-axis. However, if the disk is displaced horizontally from its equilibrium position, a horizontal restoring force F_x tends to bring the disk back to its equilibrium position. Figure 7 shows the simulated horizontal acoustic radiation force F_x that acts on the levitated disk as a function of its horizontal position x for a constant levitating height of 11.95 mm from the reflector surface. In contrast with the results of Figs. 5(a) and 6, which were simulated using the axisymmetric FEM model, the horizontal force F_x was simulated using the 3D model of Fig. 3(b), since the axial symmetry is lost when the disk is displaced along the x direction. The horizontal force of Fig. 7 has a negative slope, with a horizontal trapping stiffness k_x = 0.0372 N/m at x = 0, z = 11.95 mm.

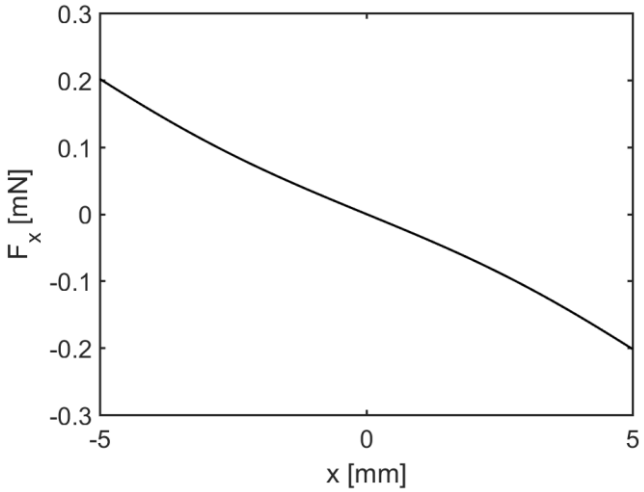

FIG. 7. Simulated horizontal acoustic radiation force F_x acting on disk as a function of the disk horizontal position for a levitating height of 11.95 mm. The radiation force was simulated using the 3D model of Fig. 3(b).

To verify the natural frequencies obtained by the FEM models, the oscillatory motion of the disk was recorded by the high-speed camera. The oscillatory motion of the disk along the x and z directions are shown in Fig. 8 [a video showing the disk oscillation is available online – Fig. 8 (Multimedia view)]. At the time instant t = 0, the voltage amplitude of the function generator was switched from 110 mV_{pp} to 130 mV_{pp}, causing the vertical equilibrium position to change from $z \approx$ 11.65 mm to $z \approx$ 11.95 mm. This change in vertical equilibrium position occurs because the trapping stiffness k_z is proportional to the voltage amplitude squared. This rapid change in the equilibrium position is followed by the damped oscillatory motion of the disk [Fig. 8(b)]. For $t > 0$, the frequencies of the horizontal and vertical oscillations were obtained by evaluating the mean period along 10 oscillations, resulting in f_x = 3.38 Hz and f_z = 18.35 Hz. These frequencies have good agreement with those obtained by the FEM models (f_x = 3.33 Hz and f_z = 19.76 Hz). In addition to the disk's oscillatory motion, we can also see in the video [Fig. 8 (Multimedia view)] that the disk rotates along the z-axis. The disk rotation seems to be caused by the viscous torque[67] induced by the acoustic streaming[68,69]. Unfortunately, our 3D acoustic model neglects acoustic streaming and it only considers the torque generated by the acoustic radiation pressure.

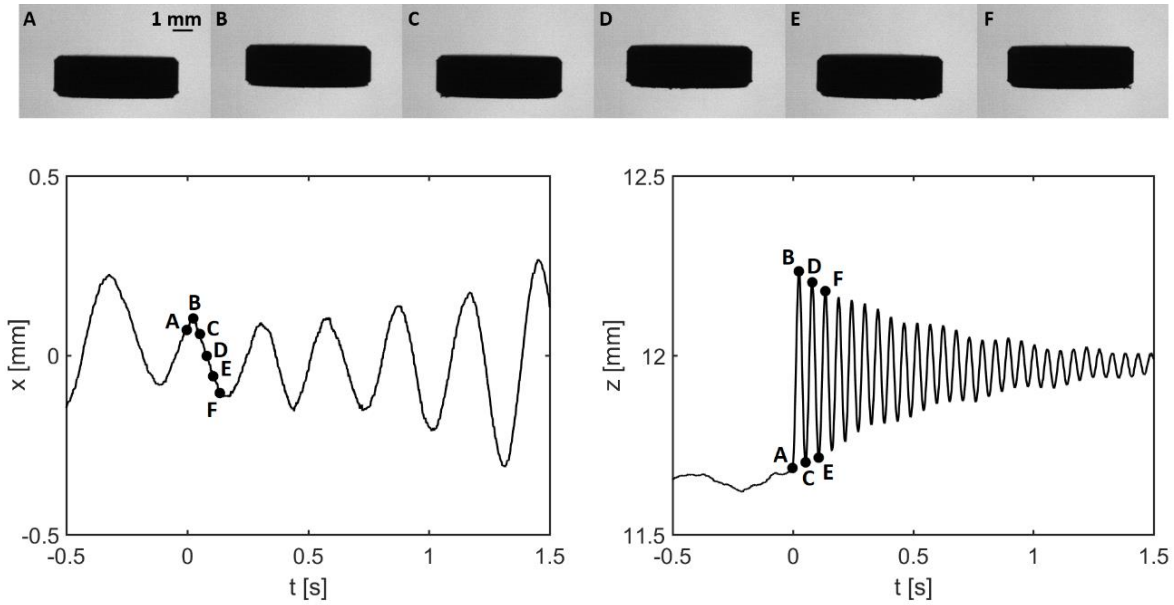

FIG. 8. Oscillatory motion of the levitating disk along the horizontal (x) and vertical (z) directions. At t = 0, the transducer voltage amplitude is rapidly switched, causing a vertical oscillatory motion. A video of the disk over time is available online. (Multimedia view).

The 3D model of Fig. 3(b) was also used for simulating the acoustic radiation torque on the disk as a function of the tilt angle θ. The disk is located at (x = 0, z = 11.95 mm) and the y-compoment of the acoustic radiation torque was simulated for θ varying between -20 and 20 degrees. The acoustic pressure distribution for θ = -20 degrees is shown in Fig. 9(a), whereas Fig. 9(b) shows the acoustic radiation torque as a function of θ. The torque curve presents a negative slope, with a torsional constant k_y^{rot} = 7.41 μN.m/rad at θ = 0. This means that when the tilt angle is altered by an external perturbation, the restoring torque causes the disk to oscillate around the equilibrium angle (θ = 0). The frequency of these oscillations can be calculated by taking into account the disk's moment of inertia I = 2.3255 x 10^{-10} kg.m^2 and then replacing k_y^{rot} and I into Eq. (10), which results in f_y^{rot} = 28.41 Hz.

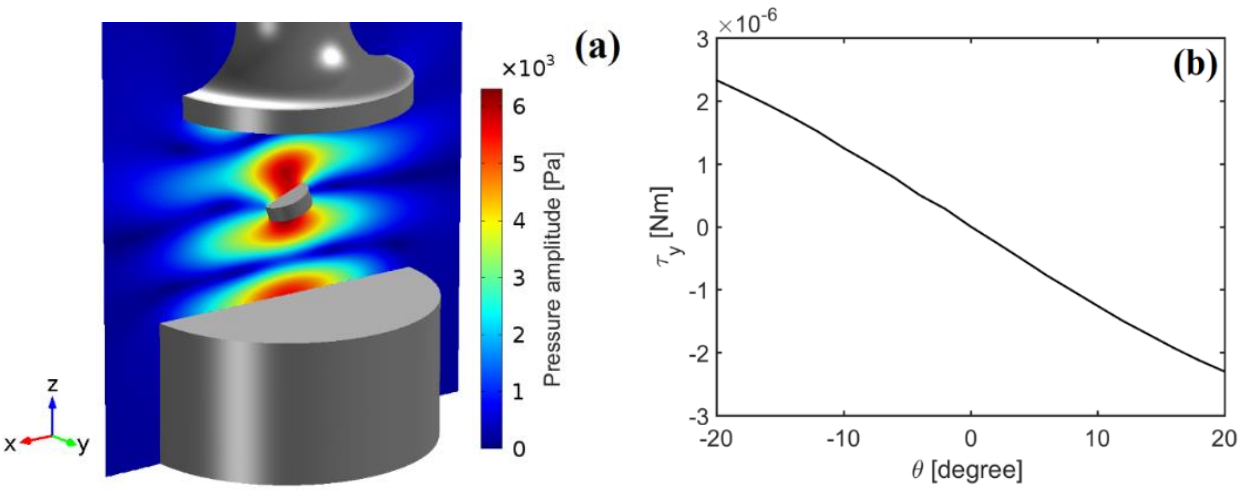

FIG. 9. Simulated results for a levitating tilted disk. The distance between the transducer and the reflector corresponds to H = 25.0 mm (third resonant mode) and u_0 = 5.6 μm: (a) Acoustic pressure distribution obtained by the 3D model when the disk is located at x = 0, z = 11.95 mm and tilted by angle θ = -20 degrees. (b) Acoustic radiation torque on the disk as a function of the tilt angle θ.

To verify the frequency obtained by the 3D model, angular oscillations of the disk are recorded by the high-speed camera. Figure 10 shows how the tilt angle θ varies with time [a video showing the angular oscillations is available online – Fig. 10 (Multimedia view)]. In this experiment the disk oscillated with a frequency of f_y^{rot} = 28.21 Hz, which is close to the frequency predicted by the model (f_y^{rot} = 28.41 Hz).

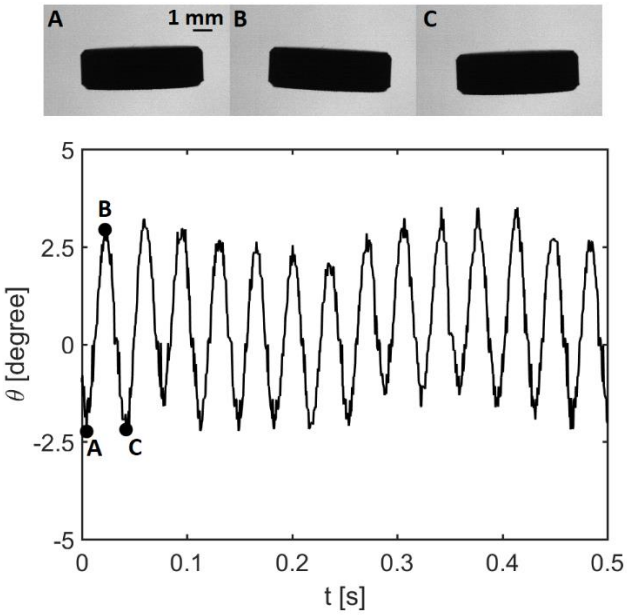

FIG. 10. Angular oscillations of the disk over time. (Multimedia view).

V. CONCLUSIONS

In this paper, we have simulated the acoustic radiation force and torque acting on a levitating disk inside a single-axis acoustic levitator. An axisymmetric model was utilized for simulating the vertical force on the disk whereas a 3D model simulated the horizontal force and the y-component of the acoustic radiation torque. In contrast with simulations based on the Gor'kov equation, which assumes that the levitating object is much smaller than the acoustic wavelength, our simulations consider the real shape of the object as well as the levitator geometry. Using the numerical models, we also calculated the trapping stiffness along the horizontal and vertical directions and the torsional constant, which were employed for calculating the natural frequencies of the vertical, horizontal and angular oscillations of the disk. The natural frequencies predicted by the models were also compared with the natural frequencies obtained experimentally, showing a good agreement between simulation and experiments. Although we have investigated the acoustic levitation of a disk, the methodology employed here can be easily extended to investigate the acoustic levitation of objects with arbitrary shapes and sizes. The methodology employed here may facilitate the design of new devices for levitating and manipulating non-spherical objects in mid-air.

AUTHOR´S CONTRIBUTIONS

All authors contributed equally to this work.

ACKNOWLEDGMENTS

The authors thank Goiás Research Foundation (FAPEG), CAPES and the São Paulo Research Foundation - FAPESP (Grant No. 17/27078-0) for supporting this research.

DATA AVAILABILITY

The data that support the findings of this study are available from the corresponding author upon reasonable request.

REFERENCES

[1] E.H. Brandt, Nature **413**, 474 (2001).

[2] R.J.K. Weber, C.J. Benmore, S.K. Tumber, A.N. Tailor, C.A. Rey, L.S. Taylor, and S.R. Byrn, Eur. Biophys. J. **41**, 397 (2012).

[3] M.A.B. Andrade, N. Pérez, and J.C. Adamowski, Brazilian J. Phys. **48**, 190 (2018).

[4] D. Zang, Y. Yu, Z. Chen, X. Li, H. Wu, and X. Geng, Adv. Colloid Interface Sci. **243**, 77 (2017).

[5] S. Santesson and S. Nilsson, Anal. Bioanal. Chem. **378**, 1704 (2004).

[6] R. Tuckermann, L. Puskar, M. Zavabeti, R. Sekine, and D. McNaughton, Anal. Bioanal. Chem. **394**, 1433 (2009).

[7] C.J. Benmore and J.K.R. Weber, Phys. Rev. X **1**, 011004 (2011).

[8] C.J. Benmore, J.K.R. Weber, A.N. Tailor, B.R. Cherry, J.L. Yarger, Q. Mou, W. Weber, J. Neuefeind, and S.R. Byrn, J. Pharm. Sci. **102**, 1290 (2013).

[9] L. Puskar, R. Tuckermann, T. Frosch, J. Popp, V. Ly, D. McNaughton, and B.R. Wood, Lab Chip **7**, 1125 (2007).

[10] T. Vasileiou, D. Foresti, A. Bayram, D. Poulikakos, and A. Ferrari, Sci. Rep. **6**, 20023 (2016).

[11] A. Scheeline and R.L. Behrens, Biophys. Chem. **165**–**166**, 1 (2012).

[12] S. Tsujino and T. Tomizaki, Sci. Rep. **6**, 25558 (2016).

[13] V. Vandaele, P. Lambert, and A. Delchambre, Precis. Eng. **29**, 491 (2005).

[14] V. Vandaele, A. Delchambre, and P. Lambert, J. Appl. Phys. **109**, 124 (2011).

[15] M.A.B. Andrade, T.S. Ramos, J.C. Adamowski, and A. Marzo, Appl. Phys. Lett. **116**, 054104 (2020).

[16] H. Bruus, Lab Chip **12**, 1014 (2012).

[17] M. Baudoin and J.-L. Thomas, Annu. Rev. Fluid Mech. **52**, 205 (2020).

[18] A.L. Yarin, M. Pfaffenlehner, and C. Tropea, J. Fluid Mech. **356**, 65 (1998).

[19] M.A.B. Andrade and A. Marzo, Phys. Fluids **31**, 117101 (2019).

[20] L. Cox, A. Croxford, B.W. Drinkwater, and A. Marzo, Appl. Phys. Lett. **113**, 054101 (2018).

[21] D. Zang, K. Lin, L. Li, Z. Chen, X. Li, and X. Geng, Appl. Phys. Lett. **110**, 121602 (2017).

[22] W.J. Xie, C.D. Cao, Y.J. Lü, Z.Y. Hong, and B. Wei, Appl. Phys. Lett. **89**, 214102 (2006).

[23] M. Sundvik, H.J. Nieminen, A. Salmi, P. Panula, and E. Hæggström, Sci. Rep. **5**, 13596 (2015).

[24] W.J. Xie and B. Wei, Appl. Phys. Lett. **79**, 881 (2001).

[25] J.K.R. Weber, C.A. Rey, J. Neuefeind, and C.J. Benmore, Rev. Sci. Instrum. **80**, 083904 (2009).

[26] M.A.B. Andrade, F.C. Buiochi, and J. Adamowski, IEEE Trans. Ultrason. Ferroelectr. Freq. Control **57**, 469 (2010).

[27] A. Dolev, S. Davis, and I. Bucher, Phys. Rev. Appl. **12**, 034031 (2019).

[28] Y. Ochiai, T. Hoshi, and J. Rekimoto, PLoS One **9**, e97590 (2014).

[29] A. Marzo, S.A. Seah, B.W. Drinkwater, D.R. Sahoo, B. Long, and S. Subramanian, Nat. Commun. **6**, 8661 (2015).

[30] A. Marzo, A. Barnes, and B.W. Drinkwater, Rev. Sci. Instrum. **88**, 085105 (2017).

[31] A. Marzo, M. Caleap, and B.W. Drinkwater, Phys. Rev. Lett. **120**, 44301 (2018).

[32] A. Watanabe, K. Hasegawa, and Y. Abe, Sci. Rep. **8**, 10221 (2018).

[33] M.A.B. Andrade, T.S.A. Camargo, and A. Marzo, Rev. Sci. Instrum. **89**, 125105 (2018).

[34] S. Inoue, S. Mogami, T. Ichiyama, A. Noda, Y. Makino, and H. Shinoda, J. Acoust. Soc. Am. **145**, 328 (2019).

[35] A. Marzo and B.W. Drinkwater, Proc. Natl. Acad. Sci. **116**, 84 (2019).

[36] M. Prisbrey and B. Raeymaekers, Phys. Rev. Appl. **10**, 034066 (2018).

[37] J. Xu, Y. Gui, and J. Ma, J. Appl. Phys. **125**, 134905 (2019).

[38] A. Marzo, T. Corkett, and B.W. Drinkwater, IEEE Trans. Ultrason. Ferroelectr. Freq. Control **65**, 102 (2018).

[39] J. Leiterer, W. Leitenberger, F. Emmerling, A.F. Thünemann, and U. Panne, J. Appl. Crystallogr. **39**, 771 (2006).

[40] J. Leiterer, F. Delißen, F. Emmerling, A.F. Thünemann, and U. Panne, Anal. Bioanal. Chem. **391**, 1221 (2008).

[41] R.H. Morris, E.R. Dye, D. Axford, M.I. Newton, J.H. Beale, and P.T. Docker, Sci. Rep. **9**, 12431 (2019).

[42] D. Koyama and K. Nakamura, IEEE Trans. Ultrason. Ferroelectr. Freq. Control **57**, 1152 (2010).

[43] D. Foresti, M. Nabavi, M. Klingauf, A. Ferrari, and D. Poulikakos, Proc. Natl. Acad. Sci. **110**, 12549 (2013).

[44] M.A.B. Andrade, F.T.A. Okina, A.L. Bernassau, and J.C. Adamowski, J. Acoust. Soc. Am. **141**, 4148 (2017).

[45] K. Melde, A.G. Mark, T. Qiu, and P. Fischer, Nature **537**, 518 (2016).

[46] G. Memoli, M. Caleap, M. Asakawa, D.R. Sahoo, B.W. Drinkwater, and S. Subramanian, Nat. Commun. **8**, 14608 (2017).

[47] R. Hirayama, D. Martinez Plasencia, N. Masuda, and S. Subramanian, Nature **575**, 320 (2019).

[48] L.P. Gor'kov, Sov. Phys. Dokl. **6**, 773 (1962).

[49] W.J. Xie and B. Wei, Phys. Rev. E **66**, 026605 (2002).

[50] N. Perez, M.A.B. Andrade, R. Canetti, and J.C. Adamowski, J. Appl. Phys. **116**, 184903 (2014).

[51] M.A. Abdelaziz and D.G. Grier, Phys. Rev. Res. **2**, 013172 (2020).

[52] E. Leung, C.P. Lee, N. Jacobi, and T.G. Wang, J. Acoust. Soc. Am. **72**, 615 (1982).

[53] F.L. Curzon and D. Plant, Am. J. Phys. **54**, 367 (1986).

[54] W.J. Xie and B. Wei, Phys. Rev. E **70**, 046611 (2004).

[55] N. Yan, W.L. Di, Z.Y. Hong, W.J. Xie, and B.B. Wei, Chinese Phys. Lett. **36**, 034303 (2019).

[56] L. V. King, Proc. R. Soc. A Math. Phys. Eng. Sci. **147**, 212 (1934).

[57] T. Schwarz, P. Hahn, G. Petit-Pierre, and J. Dual, Microfluid. Nanofluidics **18**, 65 (2015).

[58] M. Barmatz and P. Collas, Acoust. Soc. Am. **77**, 928 (1985).

[59] M.A.B. Andrade, N. Pérez, and J.C. Adamowski, J. Acoust. Soc. Am. **136**, 1518 (2014).

[60] T. Fushimi, T.L. Hill, A. Marzo, and B.W. Drinkwater, Appl. Phys. Lett. **113**, 034102 (2018).

[61] K. Hasegawa and K. Kono, AIP Adv. **9**, 035313 (2019).

[62] Z.Y. Hong, W. Zhai, N. Yan, and B. Wei, J. Acoust. Soc. Am. **135**, 2553 (2014).

[63] E. Leung, N. Jacobi, and T. Wang, J. Acoust. Soc. Am. **70**, 1762 (1981).

[64] M.A.B. Andrade, T.S. Ramos, F.T.A. Okina, and J.C. Adamowski, Rev. Sci. Instrum. **85**, 045125 (2014).

[65] M.A.B. Andrade, S. Polychronopoulos, G. Memoli, and A. Marzo, AIP Adv. **9**, 035020 (2019).

[66] J. Rudnick and M. Barmatz, J. Acoust. Soc. Am. **87**, 81 (1990).

[67] T.G. Wang and F.H. Busse, J. Acoust. Soc. Am. **69**, 1634 (1981).

[68] E.H. Trinh and J.L. Robey, Phys. Fluids **6**, 3567 (1994).

[69] K. Hasegawa, Y. Abe, A. Kaneko, Y. Yamamoto, and K. Aoki, Microgravity Sci. Technol. **21**, S9 (2009).